

## CAVITATION MODELING OF A CENTRIFUGAL PUMP IMPELLER

**Marco Antonio Rodrigues Cunha, [cunha.marco@ig.com.br](mailto:cunha.marco@ig.com.br)**  
 UFABC - Universidade Federal do ABC – Santo André – SP – Brasil

**Helcio Francisco Villa Nova, [helcio.villanova@unifei.edu.br](mailto:helcio.villanova@unifei.edu.br)**  
 UNIFEI – Universidade Federal de Itajubá - IEM - Instituto de Engenharia Mecânica - Av. BPS, 1303, 37500-903 – Itajubá – MG – Brasil

**Abstract.** *The Phenomenon of cavitation can be described as the vapor bubbles formation in an originally liquid flow, this change of phase is carried through at constant temperature and local drop pressure, generated by flow conditions. Turbo machines like centrifugal pumps suffer with loss of performance, degradation of its useful life caused by the cavitation. Under the analytical point of view the cavitation phenomenon shows very complex, bringing great physical and numerical modeling challenges. The use of tools like CFD (Computational Fluid Dynamics) has been widely used in way to get better results in projects and developments on the dynamics of fluids. With the use of CFD tools it is possible to have a forecast about the cavitation places looking for the pressure field, since the cavitation has a direct relation with the vapor pressure at the flow fluid temperature, becoming possible to add improvements in the project of the equipment in order to prevent or to minimize the phenomenon, without the use of experimental methods that in the most cases showing high cost. The main objective of this work is to present the cavitation modeling in a centrifugal pump impeller, preceded by the analysis and validation of the model applied to a planar injection nozzle, using CFD tool.*

**Keywords:** *cavitation, CFD, turbomachine, centrifugal pump impeller*

### 1. INTRODUCTION

More and more extreme operating conditions is required for equipments on industrial areas, large operating range, high performance, reliability and flexibility is required in several areas in different types of applications.

Research and evaluate best performance with safe conditions are necessary attitudes for applications and companies that wishing to go to high competitiveness. This leads us to reflect on way of improving such conditions and equipment design using CFD (computational fluid dynamics) as Yedidiah (2008). Through tools of CFD including the modeling of cavitation phenomenon is possible to explore such conditions.

Several papers have been published to model turbomachines on CFD tools. Zhou *et al* (2003), Asuaje *et al* (2005), Wongwise *et al* (2009), Yang *et al* (2011) and Dribssa *et al* (2011) shows a numerical modelization of flow in centrifugal pump using CFD codes, however, few studies take in to account the development of the cavitation phenomenon, example Zwart *et al* (2004), Bakir *et al* (2004) and Degosha *et al* (2005).

Degosha *et al* (2004) and Bakir *et al* (2005) bring up a numerical and experimental investigation of the cavitating behavior of a pump inducer showing a predict cavitation in general conformity with visualized experimentally.

Another example of paper which demonstrate a modeling of cavitation on a centrifugal pump for water pump is show by Hofmann *et al* (2001) which presents an approach three-dimensional computational comparing with experimental results for different operating conditions (flow variation). The results obtained in the analysis of centrifugal pump rotor showed a good approximation of the distribution of bubbles (cavities) obtained by numeric method when compared with the experimental results. A robust CFD methodology for predicting three-dimensional flow with extensive cavitation using Rayleigh-Plesset model is presented by Zwart *et al* (2004), with the use of the commercial code Ansys CFX, showed a good approximation too.

However, CFD results found god agreement with experimental measurements and visualization, there are some cases like vortex pump (sewage water pump) as show by Steinmann *et al* (2010) which demonstrate that the CFD results are not fully sufficient to calculate the quantitative values with required accuracy.

This paper will emphasize a cavitation model implementation on a water centrifugal pump impeller, represented by three-dimensional numerical study of steady, turbulent and incompressible flow inside the impeller passage between two blades. A grid arrangement is done and finite volume method for solving Navier-Stokes equations was used with the ANSYS CFX application.

## 2. CAVITATION AND MULTIPHASE FLOW

The phenomenon of cavitation can be described as the vapor bubbles formation in an originally liquid flow. The cavitation inception is associated with the growth of the nuclei called seed, since the real fluids on several engineering applications are not totally pure. These seeds or nuclei contain a mixture of vapor and non-condensable gases.

Once these seeds are on regions of low pressure (below the vapor pressure) the growth of seeds will occur, called cavity or bubbles. At the time these bubbles are in regions of high pressure the collapse will occur. Growth and collapse of bubbles can be described by the Rayleigh-plesset equation (9).

Although it is clear that two different streams (two fluids) can be flow with different speeds, and such relative movement is implied on separate flow study, we can use a “simplistic” hypothesis that all phases could be in theory sufficiently mixed, with dispersion, and particle size small enough in order to eliminate the relative motion between phases, this case is considered a multiphase homogeneous flow and the governing conservation equations as showed as follow:

Mass conservation for each phase

$$\frac{\partial(r_\alpha \rho_\alpha)}{\partial t} + \nabla(r_\alpha \rho_\alpha U_\alpha) = S_{MS\alpha} + \sum_{\beta=1}^{N_p} \Gamma_{\alpha\beta} \quad (1)$$

Momentum conservation for mixture

$$\frac{\partial(\rho_m u^i)}{\partial t} + \frac{\partial(\rho_m u^j u^i)}{\partial x^j} = -\frac{\partial P}{\partial x^i} + \rho_m r_\alpha g^i + \frac{\partial \tau^{ji}}{\partial x^j} \quad (2)$$

$$\tau^{ji} = \mu_m \left( \frac{\partial u^i}{\partial x^j} + \frac{\partial u^j}{\partial x^i} \right) \quad (3)$$

$S_{MS\alpha}$  is the source term of phase  $\alpha$  and  $\Gamma_{\alpha\beta}$  is the mass flow per unit of volume from phase  $\beta$  to phase  $\alpha$ . The terms  $r_\alpha, u^i, u^j, \rho_\alpha, g^i, P$  and  $\tau^{ji}$  are respectively the volume fraction of phase  $\alpha$ , Cartesian velocity components, density of phase  $\alpha$ , gravity acceleration, pressure and the stress tensor.  $\rho_m$  and  $\mu_m$  are terms of density and viscosity both of mixture.

Volume conservation is represented considering the fraction sum as unit, where  $N_p$  is the number of phases.

$$\sum_{\alpha=1}^{N_p} r_\alpha = 1 \quad (4)$$

The volume conservation equation is combined with the continuity equation to get the transported volume equation, divided by their respective phase density.

$$\sum_{\alpha} \frac{1}{\rho_\alpha} \left( \frac{\partial}{\partial t} (r_\alpha \rho_\alpha U_\alpha) + \nabla(r_\alpha \rho_\alpha U_\alpha) \right) = \sum_{\alpha} \frac{1}{\rho_\alpha} (S_{MS\alpha} + \sum_{\beta=1}^{N_p} \Gamma_{\alpha\beta}) \quad (5)$$

The above equation interpretation is simpler when consider the special case of incompressible phases with no source, simplify as:

$$\sum_{\alpha} \nabla \cdot (r_\alpha U_\alpha) = 0 \quad (6)$$

Which requires the volume flows to have a zero divergence

For the balance of volume generation due to phase change, we have:

$$\Gamma_{\alpha\beta} = -\Gamma_{\beta\alpha} \longrightarrow \sum_{\alpha=1}^{N_p} \Gamma_{\alpha} = 0 \quad (7)$$

$$\Gamma_{\alpha\beta} = \Gamma_{\alpha\beta}^+ - \Gamma_{\beta\alpha}^+ \quad (8)$$

Where  $\Gamma_{\alpha\beta}^+ > 0$  represents a positive mass flow per unit of volume from phase  $\beta$  to phase  $\alpha$ .

## 2.1. THE CAVITATION MODEL

The vapor bubble growth and collapse on liquid is ruled by Rayleigh-Plesset equation.

$$\frac{p_v - p_{\infty}}{\rho_l} = R \frac{d^2 R}{dt^2} + \frac{3}{2} \left( \frac{dR}{dt} \right)^2 + \frac{2\sigma}{\rho_l R} \quad (9)$$

For a practical CFD modeling, assuming that there are not thermal barriers to the growth and bubble collapse, neglecting the high order term, surface tension and viscosity, we have:

$$\frac{dR}{dt} = \sqrt{\frac{2}{3} \frac{|p_v - p|}{\rho_l}} \quad (10)$$

The fraction of the change of the bubble volume can be described as bellow, with the hypothesis of bubble on spherical form.

$$\frac{dV_B}{dt} = \frac{d}{dt} \left( \frac{4}{3} \pi R^3 \right) = 4\pi R^2 \sqrt{\frac{2}{3} \frac{p_v - p_{\infty}}{\rho_l}} \quad (11)$$

The fraction of the change of the bubble mass can be described as bellow.

$$\frac{dm_B}{dt} = \rho_v \frac{dV_B}{dt} = 4\pi R^2 \rho_v \sqrt{\frac{2}{3} \frac{p_v - p_{\infty}}{\rho_l}} \quad (12)$$

If there are  $N_B$  bubbles per unit volume, the vapour volume fraction can be expressed by:

$$r_v = V_B N_B = \frac{4}{3} \pi R^3 N_B \quad (13)$$

The total mass transfer on interface per unit of volume can be expressed (considering vaporization) by:

$$\dot{m}_{lv} = N_B \frac{dm_B}{dt} = \frac{3r_v \rho_v}{R} \sqrt{\frac{2}{3} \frac{p_v - p_{\infty}}{\rho_l}} = \Gamma_{\alpha\beta} \quad (14)$$

And can generalized for vaporization and condensation as:

$$\dot{m}_{lv} = F \frac{3r_v \rho_v}{R} \sqrt{\frac{2}{3} \frac{p_v - p_{\infty}}{\rho_l}} \text{sgn}(p_v - p_{\infty}) \quad (15)$$

Taking into account that the condensation occurs slowly than vaporization  $F$  is the is an empirical factor, different for condensation and vaporization and in the case of the condensation  $r_v$  have to be replaced as  $r_{nuc}(1-r_v)$ , where  $r_{nuc}$  is the fraction of nucleation points.

$$\dot{m}_v = F \frac{3r_{nuc}(1-r_v)\rho_v}{R_{nuc}} \sqrt{\frac{2}{3} \frac{p_v - p_\infty}{\rho_t}} \text{sgn}(p_v - p_\infty) \quad (16)$$

The following model parameters are used on ANSYS CFX:  $R_{nuc} = 2 \times 10^{-6} \text{m}$ ,  $r_{nuc} = 5 \times 10^{-4}$ ,  $F_{vap} = 50$ , and  $F_{cond} = 0.01$ .

For the turbulence model the standard  $k-\varepsilon$  was adopted, where  $\mu_{m\text{eff}}$  is the effective viscosity of the mixture and  $\mu_{mt}$  is the turbulent viscosity of the mixture,  $k$  is the turbulence Kinect energy per unit mass and  $\varepsilon$  is the turbulence dissipation rate.

$$\mu_{m\text{eff}} = \mu_m + \mu_{mt} \quad (17)$$

$$\mu_{mt} = C_\mu \rho_m \frac{k^2}{\varepsilon} \quad (18)$$

### 3. NUMERICAL MODEL AND DISCRETIZATION SCHEME

ANSYS CFX Solver uses the finite volume-based method, which involves spatial discretization of the domain, from the generated meshes. Three-dimensional mesh is used to build finite volumes that are used to store quantities of mass, energy, momentum, etc...

The conservation equations are integrated into each control volume, and from the Gauss divergence theorem, volume integrals are converted to surface integrals by using mathematical operators.

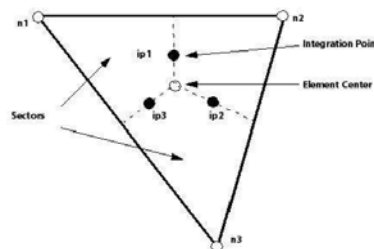


Figure 1. Mesh element example with the integration and nodes points - ANSYS CFX THEORY GUIDE, Release 13, 2010, pg 349.

On ANSYS CFX volume integrals are discretized within each sector and cumulative element to control the sector volume belongs. Surface integrals are discretized in the integration points (ipn) and the unknowns solutions are storage at the nodes (ni, mesh vertices).

The discrete conservation equations for the phasic continuity is represented as follow:

$$\frac{V}{\partial t} ((\rho_\alpha \varphi)^{n+1} - (\rho_\alpha \varphi)^n) + \sum_{ip} (\rho_\alpha u^i A^i)_{ip}^{n+1} (\varphi_{ip})^{n+1} = 0 \quad (19)$$

The advective term  $\varphi_{ip}$  requires the integration point values are approximated in terms of nodal values of  $\varphi$ . The advection scheme implemented in ANSYS CFX can be presented as below:

$$\varphi_{ip} = \varphi_{up} + \beta \nabla \varphi \cdot \Delta \vec{r} \quad (20)$$

Or on terms of volume fraction of phase  $\alpha$

$$\frac{V}{\partial t} ((\rho_\alpha r_\alpha)^{n+1} - (\rho_\alpha r_\alpha)^n) + \sum_{ip} (\rho_\alpha u^i A^i)_{ip}^{n+1} (r_{\alpha ip})^{n+1} = 0 \quad (21)$$

$$r_{\alpha ip} = r_{\alpha up} + \beta \nabla r_\alpha \cdot \Delta \vec{r} \quad (22)$$

Special choices of  $\beta$  and  $\nabla r_\alpha$  follow the high resolution scheme (for this to work).

The high resolution scheme, uses a special non-linear scheme to store  $\beta$  in each node, and calculated to be as close as possible to the value of 1 without introducing a new extreme. The advective flux is then calculated using the values of  $\beta$  and  $\nabla r_\alpha$  at the upwind node.

"The store is based on the principle used by Barth and Jespersion". (ANSYS CFX THEORY GUIDE, p372)

For pressure and velocity coupling the strategy adopted by the ANSYS CFX is by applying an apparent momentum equation for each integration point. Advective speed (mass loading) for each integration point is represented by the expression below:

$$U_{i,ip} = \bar{U}_{i,ip} + f_{ip} \left[ \frac{\partial p}{\partial x_i} \Big|_{ip} - \frac{\partial \bar{p}}{\partial x_i} \Big|_{ip} \right] - C_{ip} f_{ip} (U_{i,ip}^0 - \bar{U}_{i,ip}^0) \quad (23)$$

$$f_{ip} = \frac{d_{ip}}{1 - C_{ip} d_{ip}} \quad d_{ip} = \frac{-V}{A} \quad C_{ip} = \frac{\rho}{\Delta t} \quad (24) \quad (25) \quad (26)$$

(A) is equal to the approximation of the central momentum equation coefficient, excluding the transient term. The bars indicate the average of the adjacent values of integration point and  $^0$  is the previous values of the time step.

The phasic discretization of the momentum equation can be visualized as an evolution of the phasic equation for the velocity field.

$$\frac{V}{\partial t} ((\rho_m u^i)^{n+1} - (\rho_m u^i)^n) + \sum_{ip} (\rho_m u^j A^j)_{ip}^{n+1} (u^i)^{n+1} = - \sum_{ip} (P_{ip}^{n+1} A^i + \rho_m^{n+1} g^i V + \sum_{ip} ((\tau^{ij})^{n+1} A^j)_{ip} \quad (27)$$

With the integration of the equation (5), in the entire volume of control we define the discretized equation of pressure as shown by Zwart (2004).

$$\sum_{\alpha=1}^N \frac{1}{\rho_\alpha} \left( \frac{V}{\partial t} (\rho_\alpha^{n+1} - \rho_\alpha^n) + \sum_{ip} (\rho_\alpha r_\alpha u^i A^i)_{ip}^{n+1} - \dot{S}_\alpha V \right) = 0 \quad (28)$$

The linear system of equations is solved in ANSYS CFX using Multgrid technique created by d. Raw. (Zwart et al. 2004). The Multgrid process involves the realization of interaction in a fine mesh and later progressive interactions in virtual mesh less thin. The results are then transferred from the virtual mesh less thin to the finer original mesh.

#### 4. VALIDATION

The model validation was performed on application of an injection nozzle, shown by Roosen et al (1996) subsequently presented in studies by Yuan et al (2000) and Martynov et al. (2005). Two regimes of cavitation were stimulated and used, initial (or inlet) cavitation and supercavitation.

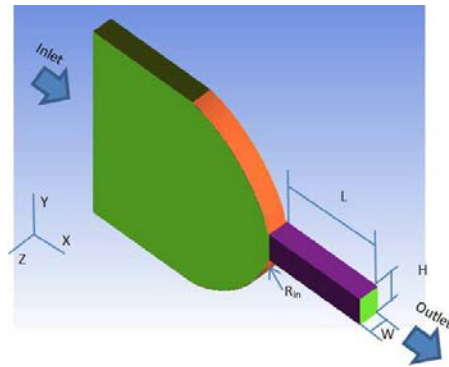


Figure 2. Main dimensions and shape of the planar nozzle presented by Roosen et al. (1996)  
Origin: Adapted from Martynov, 2005, pg 134.

The length  $L = 1$  (mm), the width  $W = 0.2$  (mm), height  $H = 0.28$  (mm) and the inner radius of curvature = 0.028 (mm). Because physical and numerical reasons, the domain was extended and the nozzle was inserted between two “reservoir” (inlet and outlet) in order to avoid flow instabilities and convergence problems.

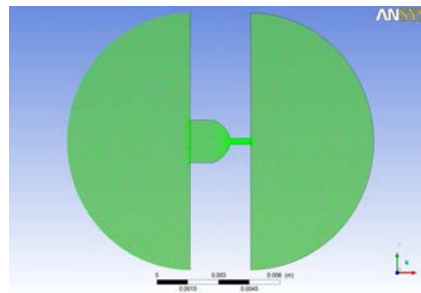


Figure 3. Extended domain modeling of injection nozzle on ANSYS ICEM with mesh, visualized on ANSYS CFX PRE.

For the reservoirs, tetrahedron elements were used with a non-structured mesh, 112410 for inlet and 108990 for outlet. The geometry and nozzle mesh was done on ANSYS ICEM and exported to ANSYS CFX Pre. For the nozzle structured hexahedron elements (73647 elements) were used and mesh refinement was done on nozzle vena contracta region.

The flow conditions of Tab. 1, was used to simulate the two cases and the boundary conditions on Tab. 2 and Tab.3, were inserted on ANSYS CFX Pre.

Table 1. Simulated flow regime with water at 25°C.

Regime	Nozzle Inlet Pressure P1, bar	Nozzle Outlet Pressure P2, bar	Velocity on Nozzle	Cavitation Number
			$U = \sqrt{2 \frac{P_1 - P_2}{\rho}}$ , m/s	$CN = \frac{P_1 - P_2}{P_2 - P_v}$
Inlet Cavitation	80	21	108,6	2,81
Supercavitation	80	11	117,5	6,28

Table 2. Boundary Conditions on reservoirs.

	Inlet Reservoir (Subdomain)	Outlet Reservoir (Subdomain)
Boundary Type	Inlet	Open
Inlet velocity	Variable	
Opening Pressure		Relative Pressure 2,1 [Mpa]
Flow Direction		Normal to the boundary
Volume Fraction	Liquid=1, vapor=0	
Type flow	Subsonic	
Turbulence	Low intensity 1%	Intensity 5%
Subdomain Conditions		
Fluid model	Isothermal Multiphase Homogeneous	
Turbulence Model	k-ε	
Liquid	Water at 300K	
Vapor	Water Vapor at 25°C	
Morphology	Both fluids continuous	
Initialization Properties		
Velocity type	Cartesian	
Static Pressure	Relative Pressure 8,1 [Mpa]	Relative Pressure 2,1 [Mpa]
Interface Domain		
Boundary Type	Interface	
Mass and Momentum	Conservative Interface Fluxes	
Turbulence	Conservative Interface Fluxes	

Table 3. Boundary Conditions on nozzle.

Nozzle	
Inlet Domain and Outlet Domain	
Boundary type	Interface
Mass and momentum	Conservative Interface fluxes
Turbulence	Conservative Interface fluxes
Conditions	
Fluid Model	Multifásico homogêneo isotérmico
Turbulence model	k-ε
Liquid	water at 300K
Vapor	Water vapor at 25°C
Morphology	both fluid continuous
Wall conditions	no-slip conditions
	roughness : smooth

The mesh was solved on a tree-dimensional form with the use of Multgrid technique.

A first approach was done on ANSYS CFX solver with the cavitation model turn off, in order to accelerate the convergence and give a preview view of points with low pressure (more susceptible to cavitation) using the velocity value of 1.55 m/s on the input boundary condition on inlet reservoir conditions giving a nozzle velocity of 108.6 m/s. The results were used on ANSYS CFX Solver as a first approach for the case with the cavitation model turn on.

The initial cavitation comparison at cavitation number  $CN = 2,81$  is show on Fig. 5 and Fig. 6.

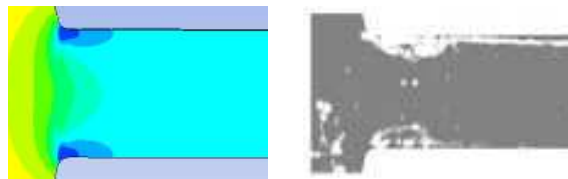


Figure 5. Qualitative comparison between the pressure field of the model applied to the ANSYS CFX and the results obtained by Roosen et al. (1996) both with  $CN = 2.81$ , density gradient, indicating the region with pressure equal to the vapour pressure, the ANSYS CFX POST (left side) approach and shadowgraph by Roosen et al. (1996) (right side).

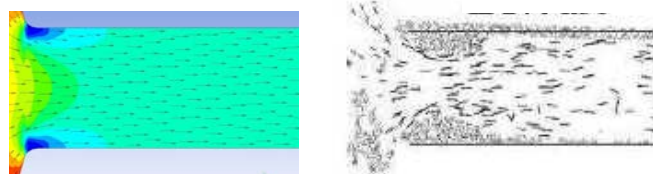


Figure 6. Vectors of velocity under conditions with the cavitation model turn on, approach of velocity obtained from ANSYS CFX POST, compared with the data obtained by Roosen et al. (1996), both with  $CN=2,81$ .

The supercavitation comparison at cavitation number  $CN = 6,28$  is show on Fig. 7.

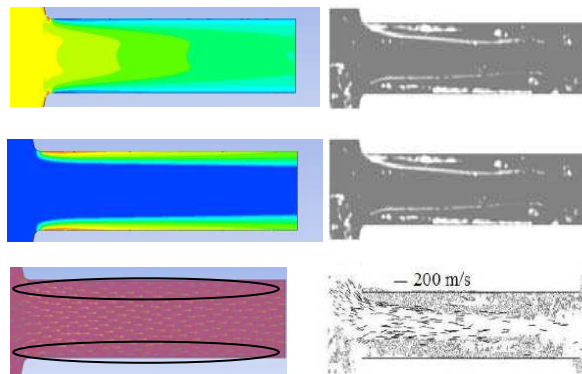


Figure 7. Pressure distribution, volume fraction and velocity vectors on supercavitation conditions with the cavitation model turned on, velocity approach from ANSYS CFX POST, compared with the data obtained by Roosen et al. (1996).

When applied the conditions of tests by Roosen et al. (1996) it was possible to have a qualitative visualization and prediction of the pressure fields for both tests (cavitation number  $CN = 2,81$  and  $6,28$ ), mainly of the regions with the value equal to or close to the saturation pressure, enabling the realization of comparative analysis with the results obtained by Rossen et al (1996). For the same cavitation number a god qualitative approach was observed for both (initial cavitation and supercavitation) cases.

## 5. Numerical model and mathematical equations for turbomachine

For turbomachine applications the inclusion of Coriolis and centrifugal forces are required. The rotation term is an intrinsic part of the acceleration and is the sum of Coriolis and centrifugal forces.

The equations of continuity and momentum in rotating coordinate can be described as below:

Continuity equation

$$\frac{\partial(r_\alpha \rho_\alpha)}{\partial t} + \nabla(r_\alpha \rho_\alpha U_\alpha) = S_{MS\alpha} + \sum_{\beta=1}^{Np} \Gamma_{\alpha\beta} \quad (29)$$

Momentum equation for turbomachine

$$\frac{\partial(\rho_m u^i)}{\partial t} + \frac{\partial(\rho_m u^j u^i)}{\partial x^j} = -\frac{\partial P}{\partial x^i} + \rho_m r_\alpha g^i + \frac{\partial \tau^{ji}}{\partial x^j} + SM \quad (30)$$

$$SM = S_{cor} + S_{cfs} \quad (31)$$

$$S_{cor} = -2\rho_m \omega \times \bar{u} \quad (32)$$

$$S_{cfs} = -\rho_m \omega \times (\omega \times \bar{r}) \quad (34)$$

Where:

$SM$  = momentum source from rotation,  $S_{cor}$  = momentum from Coriolis force,  $S_{cfs}$  = momentum from centrifugal force,

$\Omega$  = angular velocity,  $\bar{r}$  = location vector.

Rotating frames of reference (RFR) are available on ANSYS CFX-Pre. and allows the use on rotating fluid machinery such as pump impeller. ANSYS CFX-Pre enables to specify a rotating domain about axis and ANSYS CFX solver computes the appropriate Coriolis and centrifugal momentum terms.

For the numerical approach, the ANSYS CFX allows the option of multiple frames of reference that permits the analysis of situations involving domains that are rotating relative to one another.

### 5.1. GEOMETRY AND PROCESS

The impeller geometry was drawn on Autodesk Inventor as a single blade passage. A domain simplification can be done for the impeller, the axisymmetric flow option in ANSYS CFX allows modeling only a single channel, this process simplifies the modeling and computational processing time. The dimensions of the impeller are  $R_0=112$ [mm],  $R_1=71$ [mm],  $R_2=200$ [mm],  $b_1=70$ [mm],  $b_2=30$ [mm],  $\beta_1=22,5^\circ$ ,  $\beta_2=22^\circ$  and seven blades with 7[mm] thickness.

For the modeling on CFD, it is necessary to take same distance up and downstream (extension of domain), because of that, the geometry of the impeller was extended in order to allow recirculation and convergence problems.

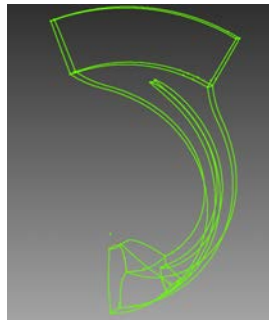


Figure 8. 3D visualization of impeller channel

### 5.2. Meshing on simulation domain

With the rotor geometry done the geometry was exported to ANSYS ICEM, a tool which enables the creation of adaptive and structured mesh in accordance with the impeller. For this study has been used structured type mesh as show below. The total hexahedron mesh number done is 21580 and 7238 quadri type.

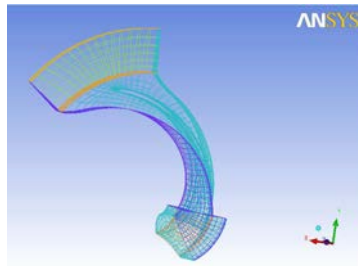


Figure 9. Channel of centrifugal pump impeller with the mesh created and visualized on ANSYS ICEM.

### 5.3. Boundary conditions and simulation parameters

The mesh and geometry was imported to ANSYS CFX Pre and the boundary conditions and simulation parameters were put on as follow.

For the operating conditions were considered the following parameters: water pumping at 25° C with isothermal model, incompressible fluid, homogeneous and steady state, mass flow in the output (output extended domain) 16 [kg/sec], model of turbulence  $k-\epsilon$ , intensity and scale of turbulence at the entrance and 0.003 0.003 respectively [m], to a constant angular speed of or 1260 [rpm], subsonic flow regime, with morphology of the fluid continues, isothermal model. The nominal head for this impeller is 34[m] for the flow of 16 [kg/sec].

For the simulation the outlet mass flow was constant and the inlet pressure variable.

In order to obtain a more fast convergence, a first convergence solution has done with the cavitation model turned off. This step is important to avoid physically impossible situation where most of flow domain is cavitating (poor initial guess). For this was inserted into the inlet boundary condition of the 100000[Pa] pressure. As well as the subsequent simulations were considered the following parameters: maximum number of 500 interactions and convergence criterion (residual) of 1e-6.

The problem was solved on ANSYS CFX solver using 1/7 of the impeller. With the use of the rotational periodic and the axis for the rotational transformation specified, it was possible represent the symmetry of the total domain.

The results of the first simulation were used as a first approach for the simulation with the cavitation model turn on using the vapor volume fraction equal 0 (considering that the vapor generation will occur in the domain).

#### 5.4. The Simulation

The simulation cases were done as showed on Tab.4.

Table 4. Cases of simulations.

n°	Inlet Pressure [Pa]	Outlet Flow [kg/s]
1	100000	16
2	80000	
3	60000	
4	40000	
5	30000	
6	25000	
7	20000	
8	18000	
9	17500	
10	16000	

Figure 10 shows preview of pressure field distributed in full view of the impeller, where it is possible to show the locations of low pressure, however, without the achievement of value of water saturation pressure at 25° C, 3574 [Pa].

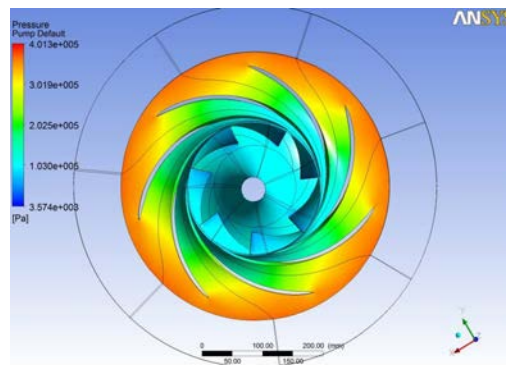


Figure 10. First approach simulation with cavitation model turned off, inlet pressure 100000[Pa] visualized on CFX Post.

The Figure 11 shows the vapor water volume fraction with the cavitation model turned on for the inlet pressure cases of 100000[Pa] – Figure A, 40000[Pa] – Figure B and 17500[Pa] Figure C. These Figures allows the visualization of the growth of vapor water volume fraction when the inlet pressure decreases.

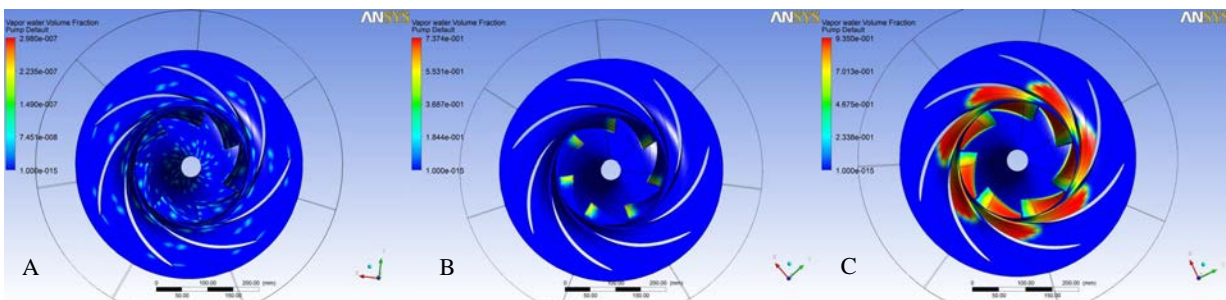


Figure 11. Vapor water volume fraction comparative (cavitation evolution) for 100000[Pa], 40000[Pa] and 17500[Pa] at inlet pressure respectively, visualized on CFX Post.

Figure 12 shows a blade to blade visualization for the pressure field for the case 17500[Pa] inlet pressure. It's possible to see places with pressure equal and above the vapor pressure value.

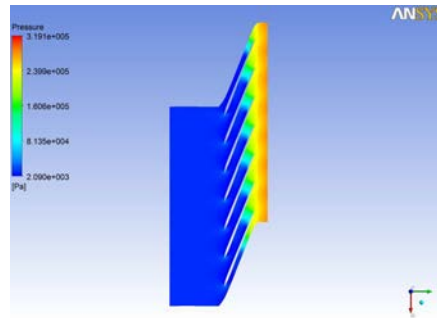


Figure 12. Pressure field Blade to Blade view for the 17500[Pa] inlet pressure condition, visualized on CFX Post.

In order to obtain parameters for the cavitation start condition in addition to the places with pressure values equal or close to the vapor pressure of water, two additional parameters related to centrifugal pumps operation have been inserted in the form of expression in ANSYS CFX Pre and allows to work with other monitoring parameters from ANSYS CFX Post results. The expressions were as follows: Head (H) and Npsh and are represented as below.

$$H = \frac{P_{outlet} - P_{inlet}}{\rho \cdot g} \tag{35}$$

$$N_{psh} = \frac{P_{inlet} - P_{vap}}{\rho \cdot g} \tag{36}$$

Where:  $P_{inlet}$  is the total pressure at inlet,  $P_{outlet}$  is the total pressure at outlet,  $P_{vap}$  is the water vapor pressure,  $\rho$  is the water density and  $g$  the acceleration gravity.

The Figure 13 shows the results and curves for Head and Npsh for the simulation, and it is possible to see the drop curve for the Head when the critical point of the cavitation is achieved (a point between 18000[Pa] and 17500 [Pa]) a drop of 3% of Head (adopted as reference by the American Hydraulic Institute) with the critical Npsh value 1,44[m] and inlet pressure 17750[Pa] called as Npsh3.

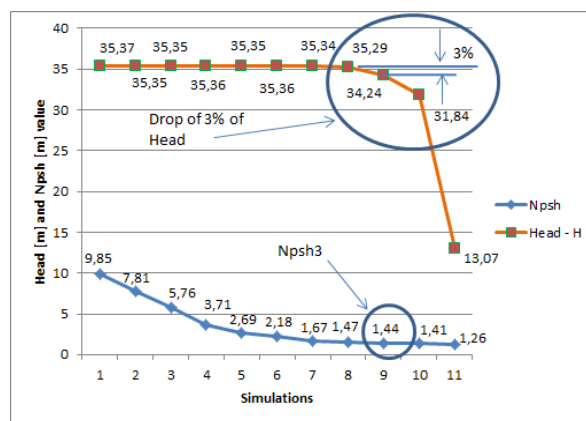


Figure 13. Diagram of Head and Npsh drop curves.

#### 4. CONCLUSION

The ANSYS CFX cavitation model has been applied with a flow in a centrifugal pump impeller as a homogenous multiphase model. The validation of the mode was first performed on an injection nozzle. In general, a good agreement was obtained about the places and format of cavities (reattachment place) in regard to the cavitation number and experimental view. For the case of the impeller it was possible to see the cavitation evolution since the inlet pressure

was modified with the increase of the vapor water volume fraction. The value for the head on simulation reach a good approach in regard to the project head.

The cavitation pockets was observed in the place that was expected (low pressure places, first on the blades inlet). With the use of monitor parameters was possible to evaluate the drop curves for Head and Npsh and was possible to see the critical point (between 18000 and 17500 [Pa]) for cavitation (the moment that the head start to drop quickly), a drop of 3% of Head (adopted as reference by the American Hydraulic Institute) with the critical Npsh value 1,44[m] and inlet pressure 17750[Pa]. Although there has not presented experimental data for the impeller, it was possible to obtain good qualitative approach for the nozzle case, showing that the use of CFD tools is a good choice to the cavitation analysis, expanding the possibilities for the phenomenon visualization.

Some important steps have to be commented, for example: The first convergence solution with the cavitation model turned off. This step was important to avoid physically impossible situation where most of flow domain is cavitating (poor initial guess) and the expansion of the domain in order to prevent convergence problems on the boundaries.

## 5. REFERENCES

- ANSYS, Inc. ANSYS CFX Introduction Manual. Release 13.0 : Canonsburg : USA, 2010.
- ANSYS, Inc. ANSYS CFD-Post User's Guide. Release 13.0 : Canonsburg : USA, 2010.
- ANSYS, Inc. ANSYS CFX-Solver theory Guide. Release 13.0 : Canonsburg : USA, 2010.
- ASUAJE, M. Numerical Modelization of Flow in Centrifugal Pump: Volute Influence in Velocity and Pressure Fields. *International Journal of Rotating Machinery*: 2005. p. 3:244-255.
- BAKIR, F.; et al. Numerical and Experimental Investigations of the Cavitating Behavior of an Inducer. *International Journal of Rotating Machinery*: 2004. p. 10:15-25.
- DELGOSHA, Coutier; et al. Numerical Simulation of Cavitating Flow in 2D and 3D Inducer Geometry. *International Journal for Numerical Methods in Fluids*: 2005. p. 48:135-167.
- Dribssa, E., Kore, S. and Aman, A., 2011, Flow Simulation and Performance Prediction of Centrifugal Pumps using CFD –tool, *Journal of EEA*, Vol.28, 2011.
- HOFMANN, M.; et al. Experimental and Numerical Studies on a Centrifugal Pump with 2D-Curved Blades in Cavitating Condition. *Fourth International Symposium on Cavitation*. California Institute of Technology: June 20-23,2001. Session B7. 005.
- MARTYNOV, S. Numerical Simulation of Cavitation Process in Diesel Flue Injectors. Thesis submitted in partial fulfillment of the requirements of the University of Brighton : United Kingdom for the degree of Doctor of Philosophy, 2005.
- ROOSEN, P.; et al. Untersuchung und Modelleirung des Transienten Verhaltens von Kavitation Serscheinungen Bei ein- und Mehrkompenentigen Kraftstoffen in Schnell Durchstromten Dusen. Report of the Institute for Technical Thermodynamics, RWTH, Aachen (Univ. of Tech.): Germany, 1996.
- Steinmann, A., Wurm, H. and Otto, A., 2010, Numerical and experimental investigations of the unsteady cavitating flow in a vortex pump, 9th International conference on Hydrodynamics, October 11-15, 2010 Shanghai, China.
- WONGWISES, S. ; CHAMAOOT, M.; KAEWNAL, S. Predicting Performance of Radial Flow Type Impeller of Centrifugal Pump Using CFD. *Journal of Mechanical Science and Technology*, Springer: 2009. p. 1620-1627.
- Yang, S., Kong, F. and Chen, B., 2011, Research on Pump Volute Design Method using CFD. Hindawi Publishing Corporation, *International Journal of Rotating Machinery*. Volume 2011, Article ID 1377860, 7 pages, 2011.
- Yedidiah, S., 2008, A Study in the use of CFD in the Design of Centrifugal Pumps. *Engineering Applications of Computational Fluid Mechanics*, Vol 2. N°3, pp 331-343, 2008.
- YUAN, W.; SAUER, J.; SCHNERR, G.H. Modeling and Computation of Unsteady Cavitation Flows in Injection Nozzle. 1st. *International Colloquium on Microhydrodynamic*, Société Française des Mécaniciens: Paris, França, 2000.
- Zhou, W., Zhao, Z., Lee, T.S. and Winoto, S.H., 2003, Investigation of Flow through Centrifugal Pump Impellers Using Computational Fluid Dynamics. *International Journal of Rotating Machinery*, 9(1): 49-61,2003.

## 6. RESPONSIBILITY NOTICE

The author is the only responsible for the printed material included in this paper.